Journal of Colloid and Interface Science 371 (2012) 1–14

Contents lists available at SciVerse ScienceDirect

Journal of Colloid and Interface Science

www.elsevier.com/locate/jcis

Feature Article (by invitation only)

Measurement and analysis of forces in bubble and droplet systems using AFM

Rico F. Tabor [a,b,*], Franz Grieser [b,c], Raymond R. Dagastine [a,b,d], Derek Y.C. Chan [b,e,f,1]

[a] Department of Chemical and Biomolecular Engineering, University of Melbourne, Parkville 3010, Australia
[b] Particulate Fluids Processing Centre, University of Melbourne, Parkville 3010, Australia
[c] School of Chemistry, University of Melbourne, Parkville 3010, Australia
[d] Melbourne Centre for Nanofabrication, 151 Wellington Road, Clayton, Victoria 3168, Australia
[e] Department of Mathematics and Statistics, University of Melbourne, Parkville 3010, Australia
[f] Faculty of Life and Social Sciences, Swinburne University of Technology, Hawthorn 3122, Australia

ARTICLE INFO

Article history:
Received 29 October 2011
Accepted 15 December 2011
Available online 27 December 2011

Keywords:
Atomic force microscope
Deformable
Drops
Bubbles
Dynamics
Surface forces

ABSTRACT

The use of atomic force microscopy to measure and understand the interactions between deformable colloids – particularly bubbles and drops – has grown to prominence over the last decade. Insight into surface and structural forces, hydrodynamic drainage and coalescence events has been obtained, aiding in the understanding of emulsions, foams and other soft matter systems. This article provides information on experimental techniques and considerations unique to performing such measurements. The theoretical modelling frameworks which have proven crucial to quantitative analysis are presented briefly, along with a summary of the most significant results from drop and bubble AFM measurements. The advantages and limitations of such measurements are noted in the context of other experimental force measurement techniques.

1. Introduction

In the quarter-century since Binnig, Quate and Gerber invented the atomic force microscope (AFM) [1], the instrument has grown to prominence as a tool for measuring nano-scale topology and interaction forces. By monitoring the bending or deflection of a micro-cantilever, information can be gained on the forces acting on the cantilever's sharp tip [2], with pico-Newton resolution. When the tip is raster-scanned over a surface, this sensitivity is used to provide a 3-dimensional reconstruction of the surface's form, down to Ångstrom (atomic) resolution.

In the early 1990s, it was demonstrated that, by attaching a colloidal particle of a few microns diameter to the end of an AFM cantilever, the force between the particle and a surface could be measured [3]. Using this method, precise information on electrical double-layer and Van der Waals forces was obtained, with specific relevance to colloidal systems [3]. Although the surface forces apparatus (SFA) [4] had previously been able to provide such insight for specific systems, the AFM offered several complementary advantages in terms of the material combinations and geometries which could be explored, no longer relying on crossed-cylinder approaches between transparent materials.

Some years later, the concept of extending the measurement of colloidal forces using the AFM to include deformable bodies emerged. The initial attempts were measurements of equilibrium forces between a solid particle on the cantilever and a bubble immobilised on a solid surface [5–8], and later between a particle and oil droplet [9–14]. However, it was soon noted that significantly more insight could be gained by picking up an emulsion-scale droplet onto the AFM cantilever [15]. This allowed interactions between pairs of droplets to be examined, where relatively high velocities could be used to explore hydrodynamic drainage effects.

The information gained in such measurements of inter-droplet collisions was underpinned by theoretical analysis [16–19]. A model had been previously developed which accounted for the force seen when a solid particle approached a deformable oil droplet, predicting the static force at any approach distance [16,20]. By introducing time as a variable, and accounting for fluid flow by lubrication theory, dynamic interactions between droplets could be modelled, which afforded major advances in understanding [17–19].

This article draws from the significant body of work pertaining to measuring interactions between soft bodies (bubbles and droplets) using the AFM. Experimental and theoretical considerations are detailed, and key outcomes and advances to date are summarised. This is relevant because of (a) velocity and deformation effects that are important in considering emulsion stability, gel interactions, and soft biological systems, and (b) film drainage studies, where the

* Corresponding author at: Department of Chemical and Biomolecular Engineering, University of Melbourne, Parkville 3010, Australia. Fax: +61 3 8344 4153.
E-mail addresses: rtabor@unimelb.edu.au (R.F. Tabor), d.chan@unimelb.edu.au (D.Y.C. Chan).
[1] Fax: +61 3 8344 4599.

0021-9797/$ - see front matter © 2012 Elsevier Inc. All rights reserved.
doi:10.1016/j.jcis.2011.12.047

displacement and its time variation are well-controlled as the (time-dependent) force of interaction is measured.

2. Scope and intention of the article

This article is intended as an introduction to techniques and theories pertaining to performing AFM force measurements specifically on soft, colloidal systems – droplets, bubbles, etc. By force measurements, we mean the determination of force *vs.* distance or force *vs.* time relationships for soft surfaces, as distinct from AFM imaging studies, which will not be covered here. It is hoped that the experimental methods and approaches detailed herein will prove useful to other researchers in this area. A summary of important results and outcomes in the field of force measurements on soft colloids provides context and motivation for the work. It is not intended as a significant review, critical or otherwise, of published work in this field in general.

Measurements of interactions (i.e., forces as a function of separation) in soft, colloidal systems have attracted much attention over recent decades. However, obtaining such information presents significant experimental and theoretical challenges, due to the effects of deformability and the often dynamic nature of colloidal systems. A number of techniques have been succesfully applied to elicit information on surface and other forces from such systems, and each approach presents its own set of advantages and limitations.

In the 1970s, the surface forces apparatus (SFA), developed by Israelachvili, Tabor and Winterton [21–23,4] enabled significant advances by measuring interactions between solid surfaces [24], successfully measuring electrical double-layer, Van der Waals, hydration and structural forces [25]. Horn applied the technique to look at interactions between a solid and a deformable interface, in the form of a drop of mercury [26,27] or an air bubble [28] squeezed from a capillary. One advantage of SFA is that by the use of an optical fringe-counting method ('fringes of equal chromatic order' or FECO), the absolute separation at any time can be known [4]. Additionally, the spatial profile of the liquid film between the approaching interfaces may be obtained, but in this case, force cannot be directly measured [26]. However, in order for this to be accomplished, material choice is limited such that the solid surface must be transparent, and almost inevitably mica in order to achieve the requisite smoothness and curvature. There are also limitations on the lateral size of interaction which must be used, requiring deformable drops or bubbles on a millimetre scale.

Interferometry was also used to study bubble–solid interactions by Fisher et al. [29,30] in experiments where a millimetre-scale bubble was blown against a silica surface, and the film profile was determined as water drained from between the air–water and solid–water interfaces. This work has recently been modelled using a dynamic lubrication theory which correctly predicts the dimpled bubble shape at initial approach [31]. The drainage of the intervening fluid between two liquid drops emerging from opposing capillaries and the deformation of the fluid/fluid interfaces have also been studied by interferometric techniques [32], and modelled with the same theoretical framework [33].

Related techniques for measuring thinning liquid films, often making use of interferometry have also been employed to explore pressures and thicknesses within thin films [34–36]. The original thin film balance work was performed by Sheludko [37] and Mysels [38]. In a typical experiment, liquid is drained from an aqueous film while pressure is simultaneously measured by a transducer and the film thickness is assessed by interferometry. In this way, the disjoining pressure as a function of film thickness is obtained. However, the films generated in such experiments are large in lateral dimensions, with very low to zero curvature.

A recent addition to the field of force-distance spectroscopy is the technique of total internal reflection microscopy (TIRM), introduced by Prieve [39,40]. In this method, a particle or droplet is held in position above a surface using an optical trap to limit its lateral (but not vertical) diffusion, and its position measured by an evanescent scattering process. Through a Boltzmann analysis, this allows a determination of the potential energy profile of the particle as a function of separation. Although limited to a small range of particle/drop sizes, forces as low as 10^{-14} N can be reliably measured.

Whilst AFM offers some useful advantages when applied to measuring force/separation relationships, there are also limitiations which must be accounted for. The most significant inherent disadvantage with AFM when specifically applied to soft matter interactions is that the absolute separation between bodies or interfaces is not explicitly known, and must be inferred. This topic is discussed in more detail in the next section, along with methods to attempt to overcome the problem.

3. Experimental equipment and methods

3.1. Equipment

3.1.1. AFM

Due to its sensitivity and precision of motion, afforded by piezoelectric elements, the AFM represents an ideal tool for analysing interactions between colloidal objects at nanometre separations. At such close approach, electrical double-layer, Van der Waals and other, more exotic colloidal forces come into play.

Although all commercial AFMs contain the same basic set of components (a cantilever combined with a laser/photodiode setup to measure its deflection, a sample stage and piezo elements to move one relative to the other, along with the necessary electronics), the design and implementation of these components differs significantly between manufacturers and models. This has naturally led to some instruments which are highly optimised for atomic-resolution imaging studies, whereas others have strong capabilites for measuring forces. In particular, instruments that have an accurate method for measuring the distance travelled by the cantilever vertically are the most suited to force measurements. The reason for this is that piezo elements tend to experience some level of non-linearity, creep and hysteresis. Hence, the expected distance of displacement for a given applied voltage at the piezo may not be precisely realised, and so the distance must be independently measured. Methods for achieving this include strain gauges, capacitive sensors within the piezos, and linear variable differential transformers (LVDTs).

AFMs may be tip-scanning instruments, where piezos are used to move the cantilever around above a stationary substrate, or sample-scanning instruments, where the sample is translated below a stationary cantilever. Practically, there is little difference in their operation, although for the measurement of force *vs.* displacement data, care must be taken to realise the correct orientation of parameters.

3.1.2. Cantilevers

The AFM cantilever is the spring, usually a few hundreds of microns long, which bends in repsonse to the forces it experiences. For measuring quantitative interactions between colloidal objects, it is clear that the colloid must be attached at a certain position, and in a measurable, reproducible way. For the attachment of solid particles, this is relatively facile, with most protocols using an epoxy resin to ensure strong attachement between the cantilever and the particle. Once attached, the particle is not free to move, and hence the properties of the cantilever-particle system (such as the optical lever sensitivty and spring constant, discussed later) can be measured.

Although initial experiments using V-shaped cantilevers offered considerable insight into the interactions between droplets, the

problem of the complex contact area that the droplets made with the cantilever did not go unnoticed. Agreement appeared reasonable, but required the assumption of a uniform contact line and a contact angle based on macroscopic measurements. In the limit of small droplet deformations, the contact angle dependence was found to be a relatively minor concern. However, to increase precision for more advanced measurements, contact areas had to be more precisely known.

To overcome this, new, custom cantilevers were designed, where the contact area of the droplet on the cantilever could be carefully controlled, allowing a much more precise knowledge of the drop geometry at all times, provided by the certainty of a pinned contact line. This was initially achieved by taking a simple rectangular beam design, of $450 \times 50\ \mu m^2$ and approximately 2 μm in thickness, fashioned from a silicon wafer by nanolithography, and adding a circular gold patch of 45 μm diameter at the end [41,42]. This patch could be chemically modified by reaction with thiols to give desired surface chemical properties. For picking up oil droplets or gas bubbles, both of which are hydrophobic in nature, a highly hydrophobic surface was required. This was achieved by adsorption of a simple alkanethiol, 1-decanethiol [42,43]. Because of the contrast between this hydrophobised patch and the hydrophilic silica (native on the silicon beam) that surrounded it, droplets and bubbles can be firmly anchored to the area described by the gold patch. An alternative design, whereby the end of the cantilever was fashioned to terminate in a circular region, slightly wider in diameter than the cantilever beam, providing a paddle-type shape, was also fabricated. This entire end region could be similarly hydrophobised, the advantage of this style being that it provides a slightly large contact area, making it easier to pick up droplets.

3.1.2.1. Sensitivity calibration. The AFM measures the deflection of the cantilever in terms of a voltage difference at the split-photodiode where the reflected laser beam is incident. To understand the physical deflection of the cantilever in distance units, this voltage must be calibrated using a value often referred to as the sensitivity, or more completely, the inverse optical-lever sensitivity (InvOLS). This can be readily measured by driving the cantilever down against a solid surface, and measuring the deflection. Once the cantilever is in contact with the solid surface, the motion of the piezo (which drives the back of the cantilever) is reflected as increasing bending (deflection) of the cantilever, measured in Volts at the photodiode. Hence, the reciprocal of the slope of this theoretically linear region, termed 'constant compliance' is taken to be the InvOLS, and is usually presented in units of nm/V.

The InvOLS can be measured in the same way if a solid particle is glued to the cantilever, but not if a bubble or droplet is attached. In the latter cases, driving against a solid surface deforms the droplet or bubble as well as bending the cantilever, and hence the slope of photodiode voltage *vs.* piezo displacement is a more complex convolution of the InvOLS with the interfacial tension, contact angle/area and radius of the droplet/bubble. Hence, for interactions between deformable bodies, the InvOLS must be measured before attachment of the colloid or after its removal (or, preferably, both to ensure consistency).

The InvOLS is dependent on the laser power, beam size, photodiode sensitivity, laser alignment on the cantilever and also on the reflective properties of the back of the cantilever. If the value is too high (more than 200 nm/V might be considered high for a force measurement), then the system is relatively insensitive to cantilever bending, and hence poor force resolution may result. Conversely, if the InvOLS is low, the range of cantilever bending measurable at the photodiode will also be low, (i.e. relatively small cantilever motion may cause the laser to be deflected out of the range of the photodiode). Depending on the spring constant, this may not allow measurement of the desired range of forces.

The InvOLS is regularly measured, and then applied as a constant value. However, this relies on the response of the optical lever system as measured at the split photodiode being linear over the range of cantilever deflections used. In the limit of small deflections, this is broadly true. However, at larger cantilever deflections (more than a few hundred nanometres), linear behaviour over the entire deflection range may no longer be obeyed, and hence the InvOLS over the entire range of experimental deflections used should be measured. If the response of the photodiode voltage *vs.* piezo motion is no longer linear, then the InvOLS should be applied as a function rather than as a constant, in order to convert voltage to deflection distance.

3.1.2.2. Spring constant. An important consideration for AFM cantilevers is the spring constant, *K*. This parameter defines how flexible the lever is, which transpires to be an important characteristic for force studies. If a cantilever is too flexible, it will deflect excessively in response to the applied force, and may no longer be detected by the laser. It will also tend to snap-in or jump-to-contact (where the force/distance gradient acting on the cantilever exceeds its spring constant) too readily in the presence of an attractive force, missing important information on force/distance relationships at close approach. Conversely, a lever which is too stiff will have very limited sensitivity to weak forces, as too great a force is required to achieve a measurable deflection. Hence, the spring constant of the cantilever must be chosen based on the expected magnitudes of force that are to be observed. For the measurement of DLVO and hydrodynamic forces between droplets and bubbles, we have found a spring constant in the region of 0.1 N/m to provide an adequate compromise between sensitivity and stiffness. Commercial cantilevers for imaging work are available with a wide range of spring constants, from around 0.005 N/m to 40 N/m or more.

For an accurate picture of the force behaviour to be obtained, it is crucial to independently measure the cantilever spring constant. It has been shown that even cantilevers taken from the same batch, fabricated from the same wafer show a variance in their spring constants of several hundred percent [44]. Due to the necessity for this information, several methods for the measurement of spring constants have emerged. Measuring the deflection against a reference cantilever of known spring constant is a very accurate method, but clearly results in a 'chicken-and-egg' problem. Cleveland suggested a method of measuring the resonant frequency of the cantilever before and after addition of a micro-scale weight [45], in the form of a tungsten sphere, although the accuracy of this method is intrinsically linked to knowing the mass of the sphere very accurately. The Sader method [46] calibrates the spring constant from the cantilever geometry, but has been shown to miscalculate spring constants for certain materials [47]. A method presented by Hutter and Bechhoeffer measures the response of the cantilever to thermal noise [48], and hence determines the spring constant assuming that it behaves as a damped harmonic oscillator. Many commericial AFMs include an automated routine for applying the Hutter and Bechhoeffer method, as it is possibly the fastest, simplest and most reliable method to obtain spring constant values.

3.2. Droplet and bubble generation, immobilisation and capture

3.2.1. Substrates for immobilisation and measuring interactions

One of the inherent problems of working with air bubbles and hydrocarbon oil droplets is that their buoyancy means they must be immobilised on a surface in order to be captured by the cantilever and studied. This presents some challenges in AFM experiments, as the surface on which they are immobilised must have a contact angle such that the droplet or bubble can be readily picked up by the cantilever. Hence, the contact area of the bubble

or droplet must be sufficient to stop it from floating away, but not greater than the contact area formed on the cantilever.

For bubbles, there are a number of methods for achieving surfaces which demonstrate the required intermediate hydrophobicity. The traditional hydrophobising agent for glass, octadecyltrichlorosilane (OTS) tends to generate surfaces which are too hydrophobic – bubbles form too large a contact area and cannot be picked up by the cantilever. However, the OTS-coated surface can be modified by partial degradation in a UV/ozone chamber for a few seconds, or by only briefly contacting them with the OTS solution (ca. 5 s) in order to decrease the surface's hydrophobicity. Resultant water contact angles between 30° and 100° have been obtained in this manner [49,42]. Recent experiments have employed an esterification reaction in ethanol to generate surfaces that are moderately hydrophobic [50,51], and suitable for temporarily tethering bubbles. The water contact angle of this surface in air is ≈40°.

When using hydrocarbon oils, the surfaces chosen are gold-coated glass substrates that have been modified by adsorption of organic thiols. By using a mixture of 1-decanethiol and 1-mercapto-1-decanol, the latter of which presents a relatively hydrophilic hydroxy terminus, a surface exhibiting the desired oil/water contact angle can be achieved [43].

When switching to certain perfluorinated oils such as perfluorooctane (PFO), this procedure becomes much simpler [52]. As PFO is significantly more dense than water, droplets readily sink, and so do not need to be pinned in place by a suitable contact area with the substrate. Here, the concern is to use surfaces which the PFO does not wet significantly, that is, the contact angle of PFO on the surface in water is as high as possible. Hydrophilic glass works well in this capacity, making fluorinated oils particularly easy to handle. Due to the hydrophobic nature of the PFO droplets, they can be readily picked up using the same thiolated gold disc cantilevers as are used for hydrocarbon oil droplets [52].

The choice of substrate used may be, in part, motivated by instrumental considerations. For the Asylum MFP-3D AFM used in the majority of our experiments, a bottom-up microscope is used to arrange and align experiments. Hence, for measuring interactions between two deformable bodies, the substrate on which the lower is immobilised must be translucent. This turns out to be only slightly limiting however, as many opaque materials such as gold, chromium, aluminum, etc. can be deposited in sufficiently thin (≈100 nm) layers such that adequate light is transmitted.

For measuring interactions between a droplet or bubble and a flat surface, a great deal more freedom is gained. There is no longer a requirement for transparency, and surfaces with any contact angle can be used. Clearly, such an experiment will often require two surfaces to be present in the AFM setup – one on which bubbles or droplets are immobilised and can be picked up from, and the surface with which interactions are to be measured. Mica is a particularly attractive surface for force measurements, as when freshly cleaved, it is atomically smooth and free from contamination. When using mica in the AFM, it is sometimes desirable to glue it in place using epoxy or clear nail polish, in order to stop it moving during the experiment.

3.2.2. Bubble generation

A reliable and reproducible method for generating bubbles using an ultrasound transducer has been developed [49,42,41,51]. In our experiments, we use ultrasound at a frequency of 515 kHz and a power at the transduction plate of 25 W. The plate is coupled to the vessel in which bubbles are to be generated with a drop of water. The vessel can be a glass Petri dish or specially-designed glass-bottomed AFM fluid cell that has been pre-functionalised as described above. Around 20–30 s of sonication is usually sufficient to provide a population of bubbles with diameters in the appropriate range (around 80–150 μm), although this depends on the solubility of the saturating gas.

In order to generate bubbles of gases other than air, solutions can be sparged, whereby the desired gas is bubbled through the solution for around 20 minutes. This displaces the air and saturates the solution with the sparging gas. Completion of the gas replacement is signalled by the solution pH: when sparging with an inert gas such as nitrogen, argon, oxygen, etc., then the pH of the solution should rise from 5.5 (when equilibrated with ambient air, due to the effect of dissolved CO_2 forming carbonic acid) to 7.0. When saturating with CO_2, the final pH should reach 3.9, signifying saturation [51].

The time-stability of bubbles is clearly of importance when measuring interactions between them using the AFM. The Laplace pressure of a 100 μm air bubble in pure water is 1.4 kPa, and hence there is a drive for it to dissolve [53]. This is more of an issue for gases with significantly higher solubilities, such as CO_2, where Ostwald ripening occurs over a few seconds when two bubbles are brought to close proximity [51]. In contrast, it is found that air bubbles do not change their size measurably over the course of our measurements (a few minutes), and if left on the cantilever, will exist for some hours. A more pressing concern when dealing with micro-scale bubbles is thermal control, as their size will change readily with even slight temperature swings. This is partially due to the expansion or contraction of the gas in the bubble, but also due to changes in gas solubility with temperature. For this reason, it is essential to ensure that the AFM and experimental solution are thermally equilibrated.

3.2.3. Droplet generation and immobilisation

For high molecular weight hydrocarbon oils, which are relatively involatile, such as C_{10} (decane) and above, droplets can be readily deposited onto a substrate by nebulising a few microlitres of the oil using a glass syringe that has been backfilled with air. The substrate then needs to be immersed in water without dislodging the droplets, which can prove problematic, as the moving contact line of water that is generated as it wets the substrate tends to gather and displace the droplets. However, Dagastine et al. developed a 'controlled dewetting' procedure, whereby water drops are carefully grown inside a teflon ring placed on the substrate (that has been decorated with nebulised oil droplets) [11]. At the line where the water drops meet, the oil droplets are deposited on the substrate underwater.

Fluorocarbon oils tend to be comparitively low boiling (e.g. PFO has a boiling point of 103°), and hence the droplets made by nebulising the oil in air over the substrate evaporate in seconds. Instead, forming the droplets directly under-water is appropriate, and can be achieved by back-filling a glass syringe with a few microlitres of oil and a few hundred microlitres of water [52]. Discharging this mixture provides a coarse emulsion with a distribution of droplet sizes, including those appropriate for AFM measurements. Because fluorinated oils tend to be more dense than water (PFO has a density of 1.77 g/cm^3), the droplets settle to the bottom, and hence attachment is not an issue as with hydrocarbon oils, which are invariably lighter than water.

3.2.4. Capturing droplets and bubbles on the AFM cantilever

In order to measure the interaction between pairs of droplets, or between a droplet and solid surface, a droplet must first be captured onto the AFM cantilever. Several approaches have been developed [54,11,43] with increasing degrees of complexity. The simplest is achieved by using the optical microscope to align the end of the cantilever over a suitably sized droplet or bubble, and then using the AFM motion control to bring the cantilever down until it contacts the droplet. Provided the AFM cantilever has been functionalised to provide a suitably hydrophobic surface for the droplet, raising the cantilever should cause the droplet to detach from the surface. In some cases, lateral translation of the cantilever

or substrate during this process can be advantageous, as the moving contact line of the droplet on the surface may 'peel off' more easily than for a directly vertical lift. The same procedure is used also for bubbles, and is shown schematically in Fig. 1

3.3. Benefits and complications of working with deformable bodies

Bubbles and droplets provide many advantages over solid probes, not just for the case that one wishes to explore interactions between them. They can also be used as probes for the surface properties of other materials. In this capacity, they offer an unique and vital characteristic: when experiencing a repulsive force, a droplet or bubble will deform, increasing its effective area of interaction to many times greater than that of a hard sphere at close approach. This increased interaction area provides greater sensitivity, and a more reliable and reproducible method for measuring such interactions. In addition, droplets and bubbles are exceptionally smooth, far smoother than the cleanest and least rough spheres, and hence can reliably achieve smaller separations and probe weaker forces than their rigid counterparts, provided the Laplace pressure permits. Droplets and bubbles also offer a wide range of options for controlling Van der Waals forces, to provide net repulsive or attractive interactions with solid surfaces, and to enhance or minimise the Van der Waals attraction between like pairs of droplets or bubbles in water.

However, their inherent deformability raises challenges: when a solid particle is used as a probe, its position at all cantilever-surface separations can be known, by measuring the point of hard contact. As a droplet or bubble can deform in response to the forces it experiences, there is often no contact, and hence the separation is not clearly defined. Approaches to deduce the separation between deformable bodies and surfaces, and between pairs of droplets or bubbles rely on a combination of theoretical models and experimental measurements (discussed below).

In addition, under certain circumstances, bubbles and droplets may coalesce when an attractive force dominates, and at sufficiently close approach. This property is unique to deformable systems, and is clearly of interest in systems where it is desirable to break an emulsion or foam to cause a bulk separation. However, it also means that post-coalescence, no more interactions can be measured between the two bodies, and hence another pair of droplets or bubbles must be found and scrutinised.

A final issue is that drops and bubbles are by their nature dynamic entities. The curvature of their interfaces means that their internal Laplace pressure favours dissolution or Ostwald ripening, and hence their size may not be stable over the course of an AFM measurement, depending on its timescale. For fluorocarbon oils, whose water solubility is vanishingly low [55], ripening is immeasurably slow, and hence of no concern for even the smallest drops. For hydrocarbon oils of C_{10} and greater, their low aqueous solubilities also means that ripening is sufficiently slow to be of no concern in a typical AFM meausurement. Bubbles of moderately soluble gases (such as nitrogen, oxygen, argon) of around 100 μm will typically dissolve slowly enough to be considered stable over several minutes, allowing most AFM measurements to be completed with little concern. However, small bubbles (<30 μm), which have much higher internal Laplace pressures, dissolve much more quickly, and will change their size over a few tens of seconds. When using highly soluble gases such as CO_2, ripening occurs in the bulk very rapidly, and is particularly problematic during the close approach of two bubbles, where for 100 μm bubbles, their radii will change significantly in a few seconds, making slow measurements impossible. A useful protocol is to measure the bubble radii microscopically before and after a measurement. If the agreement is poorer than a few μm, then the radii cannot be considered to be static throughout the measurement, and the data will be poorly defined.

4. Results and revelations

4.1. Equilibrium measurements – colloidal forces

4.1.1. Modelling framework

In the operation of the AFM as discussed in section B and Fig. 2a, the relative displacement, *Z*, of the cantilever is set by the piezo motion, and measured independently by some means. In the case of the Asylum MFP-3D that we often use, the displacement is measured by a linear variable differential transformer, LVDT. The deflection of the cantilever, *S*, is measured by the optical lever, and the interaction force, *F*, can then be obtained using the cantilever spring constant, *K*, via Hooke's Law: $F = KS$.

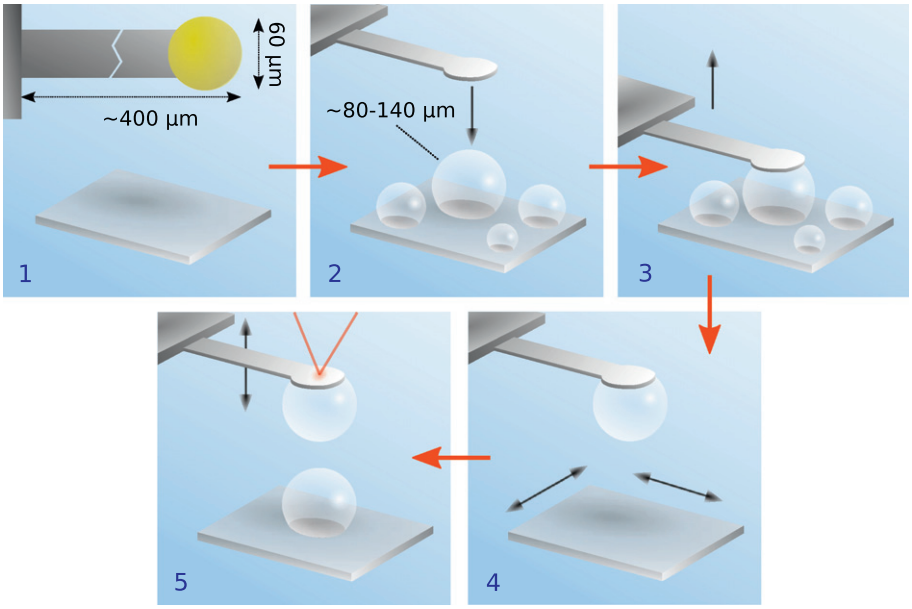

Fig. 1. Schematic diagram showing how bubble or drop pair interactions are arranged in the AFM.

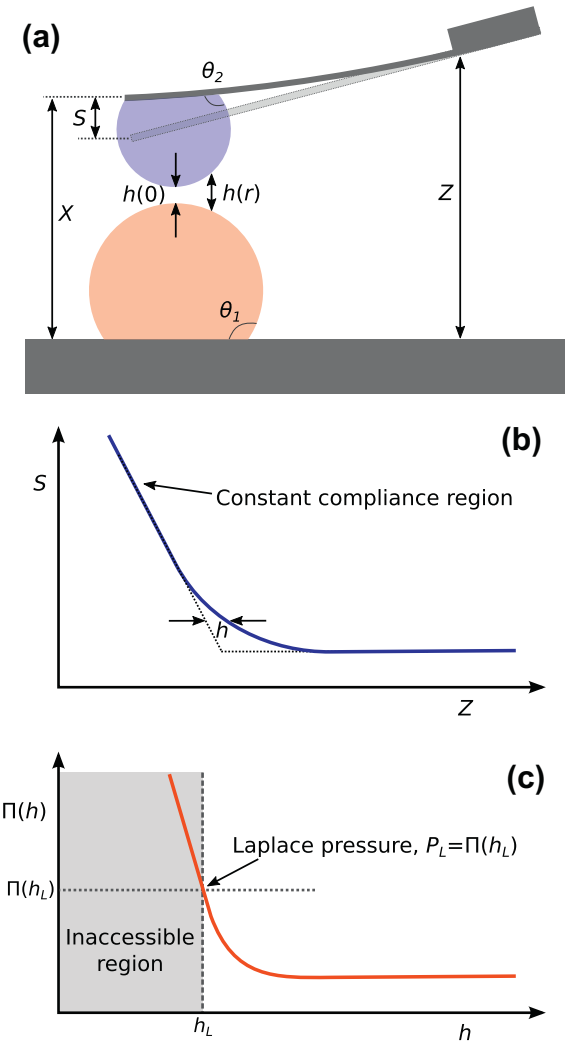

Fig. 2. A schematic diagram of the atomic force microscope that illustrates the relation between the relative piezo displacement, Z, of the cantilever, the cantilever end position, X, and the cantilever deflection, $S = F/K$, which is related to the interaction force, F, and the cantilever spring constant, K. (b) Schematic relation between the relative piezo displacement, Z, and the cantilever deflection, S, for a repulsive interaction between two rigid bodies. (c) An illustration of the inaccessible region of the repulsive disjoining pressure between a particle and a deformable bubble/drop delineated by the Laplace pressure.

A quantitative force measurement experiment seeks to determine the relationship between the force, F, and the separation, h, between two interacting bodies as the displacement, Z, is varied. In the surface forces apparatus, the change in separation, δh, can be measured with sub-nanometre resolution by monitoring changes in the wavelength of interference fringes. However, surface areas of $\approx$100 μm in the lateral direction are required, and at least one of the materials must be transparent. These conditions are not required in the AFM apparatus.

The determination of the separation in AFM force measurements is relative to the 'hard contact' position. After two rigid interacting bodies are brought into contact, any further decrease in the Z distance must result in a corresponding proportionate change in the measured cantilever deflection, S (see Fig. 2b). This region of linear relationship between S and Z, is called the constant compliance regime. The value of Z that corresponds to zero separation, or more precisely, to the reference value $h = 0$, is the hard contact position.

On the other hand, when one or both interacting bodies are deformable, a direct experimental determination of the position $h = 0$ becomes problematic. Consider the simple example of a solid spherical colloidal probe on the cantilever interacting with a deformable bubble (or drop) on the substrate shown in Fig. 2a. Assume the interaction between the particle and the bubble is given by a monotonically increasing repulsive disjoining pressure, $\Pi(h)$, with decreasing separation (see Fig. 2c). As the particle is pushed towards the bubble, the separation h will decrease but the extent of the deformation of the bubble will also increase. When the separation reaches the value h_L, at which $\Pi(h_L) = P_L$, the Laplace pressure of the bubble, further approach of the particle towards the bubble will only result in deformations of the bubble surface, causing it to 'wrap' around the particle while maintaining a constant separation (film thickness), h_L. As a result of this bubble deformation, the region $0 < h < h_L$ cannot be accessed in a force measurement experiment in which a film is maintained between the bubble and the particle (see Fig. 2c). We assume that the film between the bubble and the particle remains intact. If this film ruptures, the force measurement experiment becomes a capillary wetting phenomenon.

Therefore, after reaching $h = h_L$, instead of a constant compliance region with a simple linear relation between the displacement, Z, and the deflection, S, as the particle is pushed towards the bubble, the $S - Z$ relation will be more complex because of the deformation characteristics of the bubble. Indeed, the magnitude of the interaction force depends on the deformed shape of the bubble and the extent of bubble deformation depends on the local pressure acting on the bubble interface. Therefore the force between the particle and the bubble, and the deformation of the bubble need to be determined consistently.

In the first equilibrium AFM force measurements between a particle and a bubble [5–7], the deformational response of the bubble was assumed to be that of a Hookean spring. The effective spring constant of the bubble and hence the reference $h = 0$ for the separation is deduced from the apparent constant compliance region in the experimental results. However, it has been pointed out that this approach can give very misleading results for the disjoining pressure and should not be used [56].

For interactions between rigid bodies whose geometric shape is known, the Derjaguin construction can be used to deduce the force from the interaction free energy per unit area between parallel half-spaces of the same material. While the approach is valid only if the range of the force is small compared to the characteristic radius of curvature of the bodies, this requirement is met in most applications. However, for deformable bodies such as bubbles/drops, the shapes of the bubble/drop interfaces are not known *a priori* because the interfaces deform as a result of surface force or stresses. Such changes in the interfacial geometry will in turn affect the total force between the interacting bodies. Therefore a quantitative description of the interaction between deformable bodies is more complicated because of the need to treat variations of the force and deformation with relative displacement in a consistent manner.

A detailed analysis of the equilibrium force, F *vs.* the relative cantilever end position, ΔX, for the interaction between a particle and a bubble/drop in the AFM context, in which the bubble/drop deformation was described by the solution of the Young–Laplace equation was given by the Chan–Dagastine–White model [16,20]. Consider a bubble whose deformability is characterised by the interfacial tension, σ, and unperturbed radius R_b. Given the disjoining pressure, $\Pi(h(r))$ acting between the particle and the bubble surface, and assuming the interaction geometry is axially symmetric, a condition fulfilled in AFM experiments, the solution of this problem is given parametrically in terms of the central separation of the film, $h_0 = h(r = 0)$ (see Fig. 2a):

$$\Delta X = h_0 + H(h_0) + \frac{F(h_0)}{4\pi\sigma}\left[\log\left(\frac{R_p h_0}{4R_b^2}\right) + 2B(\theta)\right] \quad (1)$$

where

$$F(h_0) = 2\pi\int_0^\infty \Pi(h) r dr \quad (2)$$

and

$$H(h_0) = \frac{1}{\sigma}\int_0^\infty \Pi(h) r \log(r) dr \quad (3)$$

The film thickness, $h(r)$ between the particle of radius, R_p and the bubble is found by solving (numerically) the Young–Laplace equation:

$$\frac{\sigma}{r}\frac{d}{dr}\left(r\frac{dh}{dr}\right) = 2\sigma\left(\frac{1}{R_p}+\frac{1}{R_b}\right) - \Pi(h) \quad (4)$$

with the boundary conditions at $r = 0$:$h = h_0$, $dh/dr = 0$ and

$$h(r) \to h_0 + \frac{r^2}{2}\left(\frac{1}{R_p}+\frac{1}{R_b}\right) + H(h_0) - \frac{F(h_0)}{2\pi\sigma} \quad \text{as } r \to \infty \quad (5)$$

The expression for the term $B(\theta)$ in terms of the unperturbed contact angle, θ, depends on the assumed behaviour of the three phase contact line of the bubble on the substrate during interaction. The cases considered are either that the contact line is pinned (and the contact angle changes) or the contract angle remains constant (and the contact line is free to move along the substrate):

$$B(\theta) = 1 + \frac{1}{2}\log\left(\frac{1+\cos\theta}{1-\cos\theta}\right) \quad \text{(pinned contact line)} \quad (6)$$

$$B(\theta) = 1 + \frac{1}{2}\log\left(\frac{1+\cos\theta}{1-\cos\theta}\right) - \frac{1}{2+\cos\theta} \quad \text{(constant contact angle)} \quad (7)$$

The algebraic errors in the original expressions [16] for $B(\theta)$ were corrected by Bardos [57].

If the disjoining pressure, Π is repulsive and the film thickness is close to h_L, where $\Pi(h_L) = P_L$ (the characteristic Laplace pressure), a general but non-linear relation between the force, F, and relative changes in the cantilever end position, ΔX (see Fig. 2a) can be derived for the particle-bubble interaction [19] with $R' = (1/R_b + 1/R_p)^{-1}$

$$\Delta X = \frac{F}{4\pi\sigma}\left[\log\left(\frac{FR'}{8\pi\sigma R_b^2}\right) + 2B(\theta) - 1\right] \quad (8)$$

A similar expression between the relative cantilever end position, ΔX and the force, F can also be derived for the interaction between two dissimilar bubbles/drops:

$$\Delta X = \frac{F}{4\pi\sigma_1}\left[\log\left(\frac{FR_h}{8\pi\sigma_h R_1^2}\right) + 2B(\theta_1)\right] + \frac{F}{4\pi\sigma_2}\left[\log\left(\frac{FR_h}{8\pi\sigma_h R_2^2}\right) + 2B(\theta_2)\right] - \frac{F}{2\pi\sigma_h} \quad (9)$$

where R_h and σ_h are defined in terms of the unperturbed radii (R_1, R_2) and interfacial tensions (σ_1, σ_2) as:

$$\frac{1}{R_h} = \frac{1}{2}\left(\frac{1}{R_1}+\frac{1}{R_2}\right) \quad \text{and} \quad \frac{1}{\sigma_h} = \frac{1}{2}\left(\frac{1}{\sigma_1}+\frac{1}{\sigma_2}\right) \quad (10)$$

These approximate relations between F and ΔX can provide rapid verification that experimental force results are consistent with known system properties. The non-linear nature of these relations underscores the earlier observation that the deformations of bubbles/drops should not be treated as Hookean springs [56].

When the disjoining pressure as a function of separation has regions of repulsion and attraction with a sufficiently steep gradient, the resulting force-displacement relation can exhibit hysteretic effects between when deformable bodies are being brought together and when they are being separated. We will consider practical manifestations of such effects in Section 4.1.3. One final technical point to note is that these results assume the extent of the deformation remains small compared to the characteristic dimensions of the bubble/drop [19].

4.1.2. DLVO forces: electrical double-layer and Van der Waals interactions

The Derjaguin–Landau–Verwey–Overbeek (DLVO) theory was developed as a method for understanding and explaining the stability (or lack thereof) of dispersions of colloidal particles [25,53]. The method accounts for both the electrical double-layer force – due to interactions of overlapping ionic atmospheres near charged surfaces – and the Van der Waals force, an ubiquitous interaction between all materials, the magnitude of which depends on the dielectric repsonses of the materials involved. Since its inception, it has been applied successfully to understand interactions within a vast range of colloidal systems, including emulsions and foams.

In AFM experiments, as force is often readily measured as a function of separation, the DLVO theory can be (and has been) widely tested. In most colloidal systems studied by AFM, particlarly in earlier particle *vs.* plate geometries, 'classical' DLVO behaviour is observed at separations of more than a few nanometres [3,58,59], whereby interactions can be explained by fitting the correct surface charges, ionic strength and Hamaker constant or function. At separations of a few nanometres or less, other surface forces may mask the expected behaviour from DLVO theory, particularly the short range hydration repulsion [3] or hydrophobic attraction [58], also noted in SFA experiments [24,60,61]. The hydration repulsion has been especially noted for silica, which has a strongly hydrated surface, and retains strongly-bound water molecules [62]. Due to this bound water, a very strong, short-range repulsion is seen at separations below around 3 nm [3,61]. Similarly, if two hydrophobic surfaces are brought to within a few nanometres, an entropic force due to the preferred orientation of water molecules at such hydrophobic surfaces may act as a strong attraction [60,63,64], first rigorously explored by Blake and Kitchener [65]. However, the existence of this force is much harder to measure, as it is almost always masked by a longer-range Van der Waals attraction.

It is important to distinguish this short-range hydrophobic force from the suggested 'long-range hydrophobic force' [66]. The existence and origin of this latter interaction has been much debated over recent years [67,68]; it has been observed between hydrophobised solid surfaces in water [69], and occurs at separations and magnitudes greater than the Van der Waals force. Explanations have included cavitation of bubbles in the gap between surfaces [70], long-range structuring of water molecules [71], surface-adsorbed nanobubbles and bridging bubbles [72]. It is interesting to note that despite their inherent hydrophobicity, we have never observed such a force between oil droplets or gas bubbles, suggesting that the phenomenon is only seen between solid surfaces.

By measuring interactions between pairs of gas bubbles or oil droplets using the atomic force microscope, information on the electrical double-layer and Van der Waals forces acting between them has been gained. As a consequence of their deformability, in the presence of a repulsive force, droplets and bubbles flatten to extend their area of interaction, making them more sensitive probes for weak forces than, for example, solid spheres.

The strength of the Van der Waals interaction between bodies is related to the difference in their dielectric response (a good indicator of which is their refractive indices, n_D^{20}) [25,53]. Two identical materials interacting through a third material, or through a vacuum, will always experience an attraction, the strength of which increases for larger differences between refractive indices. Hence, two air bubbles ($n_D^{20} \approx 1$) in water ($n_D^{20} \approx 1.33$) experience a much

stronger attraction than do two tetradecane droplets ($n_D^{20} \approx 1.43$) in water. An important consideration is the effect of solution ionic strength on the Hamaker function. The first term (so-called 'zero-frequency' term) in the Lifshitz summation used to calculate Hamaker functions contains contributions from Keesom and Debye dipolar interactions. Hence, this term is particularly important when dealing with water, due to its very high relative static permittivity (80 at 293 K). For material combinations in which the difference in refractive indices is small, such as tetradecane and water, the zero frequency term can be a relatively significant proportion of the total value of the Hamaker constant or function. In salt solutions, this term decays exponentially with separation, with twice the Debye length as the characteristic screening parameter. Hence, for Hamaker functions and constants for such material combinations involving water, it is important that the calculation takes into account ionic strength. Table 1 provides Hamaker constants for some material combinations that are commonly-encountered in soft-matter interactions.

The Van der Waals force is short-ranging in nature, decaying as a function of separation cubed [79,25]. This decay is exacerbated by retardation – effects due to the finite speed of light limiting the correlation of electronic dipole moments in the visible and UV spectrum. Hence, the often-quoted Hamaker 'constant' for a given combination of materials is really only accurate at near-zero separations. At greater distances, this value will be smaller in magnitude for interactions between identical materials, and a Lifshitz calculation may be used to calculate the true interaction parameter at any separation [79]. The effects of retardation of the Hamaker function for hard materials were first demonstrated using SFA [22] and later using AFM [80] and TIRM [81], demonstrating that retardation is readily experienced using sufficiently sensitive force measurements. We have noted a similar level of sensitivity when dealing with bubble systems at their isoelectric point [51]. Recently, it was shown that for asymmetric air–water–oil interactions, the sign of the Hamaker function could be changed by salt screening effects, and that the functional form shows a complex separation-dependence [82], seen as the long-dashed line in Fig. 3. This is strong evidence that in some situations, a separation-dependent function is much more appropriate to model interactions than a constant, particularly for combinations of three (or more) dissimilar materials. It is only comparatively recently that sufficiently sensitive force-measuring devices have become available, such that accurate distinction between retarded Hamaker functions and Hamaker constants can be realised experimentally. Fig. 3 shows a selection of retarded Hamaker functions for material combinations commonly encountered when working with air bubbles.

Surfaces and interfaces tend to spontaneously acquire adsorbed or bound surface charges when immersed in water, the sign and magnitude of which may be linked to their surface chemistry [53]. These charges attract a swarm of excess counterions via the balance of entropy and the Coulomb force to form the diffuse layer, and these two layers in consort comprise the electrical double-layer. When two thusly charged surfaces are brought into close proximity, the overlap of diffuse layers will give rise to an attraction or repulsion, depending on the magnitude and sign of the surface charges [25,53].

It has been seen that for gas bubbles and oil droplets, the surface charge almost certainly arises from adsorption of ions from solution, and that in water, these are dominated by hydroxide ions or protons [83,84]. Measurement of the surface charge on bubbles and droplets has been achieved independently by electrophoresis [84,85] and AFM [51,82], with excellent agreement. Surface potentials derived from AFM experiments with bubbles and droplets are shown in Fig. 4. At both the air–water and oil–water interfaces, adsorption of hydroxide appears to be preferential, with an apparent isoelectric point (iep) at around pH 2.5–3 for inert gas bubbles and oil droplets [51,82]. It is noted that the presence of CO_2 in bubbles of air or pure CO_2 strongly influences the equilibrium surface charges attained, most likely through the carbonic acid equilibria [86] set up by dissolving CO_2. Hence for air bubbles, the iep is at around pH 4, and for CO_2 bubbles, close to pH 7.

It is important to note that, because the interaction force between bubbles and droplets is sensitive to repulsive disjoining pressures which are linked to film thicknesses [18], the surface potentials measured by AFM are most accurate at low surface charges. At higher charges, where the double-layer interaction maintains a much thicker film, sensitivity to variations in surface potentials is inherently lower, and hence electrophoresis can be complementary by providing increased accuracy in these extreme regions [84,85]. However, an inherent benefit of AFM when used to probe interactions between pairs of droplets is that more information can be

Table 1
Some Hamaker constants, in units of 10^{-21} J, for material combinations including tetradecane (TD), perfluorooctane (PFO), polystyrene (PS) and other substances. These were obtained by Lifshitz calculations, and represent the limiting value at a separation of 0.1 nm. For combinations involving water, the calculation was performed using three different representative dielectric spectra for water [73–75], in order to demonstrate the impact of this aspect on the eventual value arrived at. The dielectric construction for TD and PS were from Prieve and Russel [76]; those for silica and mica were from Bergström [77]; gold was from Parsegian and Weiss [74]; heptane was from Hough and White [75]. The construction for perfluorooctane was estimated by a linear extrapolation of the UV and IR oscillator strengths and static permittivity from the data given for C_5–C_7 perfluorocarbons in the work of Drummond et al. [78]. The ionic strength of water at pH 7 was used.

Material combination	Hamaker constant for water construction[a]		
	DPW (10^{-21} J)	PW (10^{-21} J)	HW (10^{-21} J)
Air–water–air	55.4	38.3	36.1
TD–water–TD	7.80	4.83	4.90
Heptane–water–heptane	6.88	3.86	3.95
PFO–water–PFO	6.99	3.75	3.99
SiO_2–water–SiO_2	6.17	7.47	8.41
Mica–water–mica	13.2	19.3	21
Gold–water–gold	489	536	544
Alumina–water–alumina	33.8	47.1	50.2
PS–water–PS	12.3	13.3	14.0
Air–water–TD[b]	8.00	−2.26	−3.39
Air–water–heptane[b]	10.0	−0.19	−1.28
Air–water–PFO	16.0	5.65	4.65
Air–water–SiO_2	−1.14	−9.22	−9.87
Air–water–mica	−15.4	−21.0	−21.3
Air–water–gold	−150	−129	−124
SiO_2–water–TD	6.09	5.17	5.67
SiO_2–water–heptane	5.32	4.46	4.97
Gold–water–TD[c]	−10.6	16.6	22.2
Gold–water–heptane[c]	−17.7	9.69	15.3
PS–water–TD	7.92	6.87	7.24
PS–water–heptane	6.48	5.45	5.87
TD–air–TD	47.1		
Heptane–air–heptane	42.4		
PFO–air–PFO	31.2		
SiO_2–air–SiO_2	63.8		
Mica–air–mica	97.2		
Gold–air–gold	667		
Alumina–air–alumina	149		
PS–air–PS	77.3		

[a] DPW – Dagastine, Prieve and White [73]; PW – Parsegian and Weiss [74]; HW – Hough and White [75].
[b] Because of the large effect of the zero frequency term from the different water constructions [76], the Hamaker function for these combinations is particularly sensitive to salt, with changes in both magnitude and sign occurring when changing water construction or ionic strength. For these reasons, use of a static Hamaker constant for these combinations is not recommended.
[c] Overlap of the low-frequency terms of the DPW water construction with the dielectric spectrum of tetradecane causes a sign reversal at short separations that is not reflective of the entire Hamaker function.

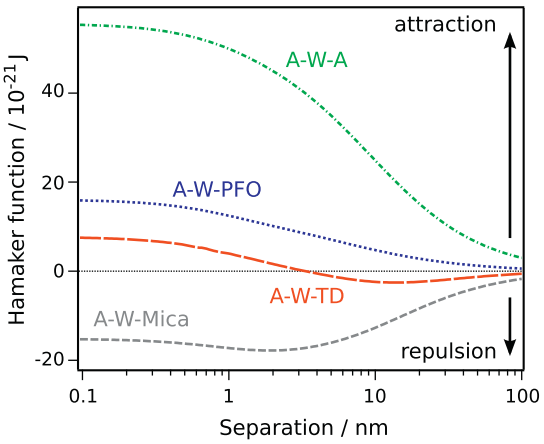

Fig. 3. Hamaker functions for common material combinations involving air (A) and water (W), calculated for an effective salt concentration of 0.1 M, by means of a Lifshitz summation [76,79]. The dielectric construction for tetradecane and mica were from Prieve and Russel [76] and Bergström [77] respectively. The construction for perfluorooctane was estimated by a linear extrapolation of the UV and IR oscillator strengths and static permittivity from the data given for C_5–C_7 perfluorocarbons in the work of Drummond et al. [78] The construction for water user here was from Dagastine et al. [73].

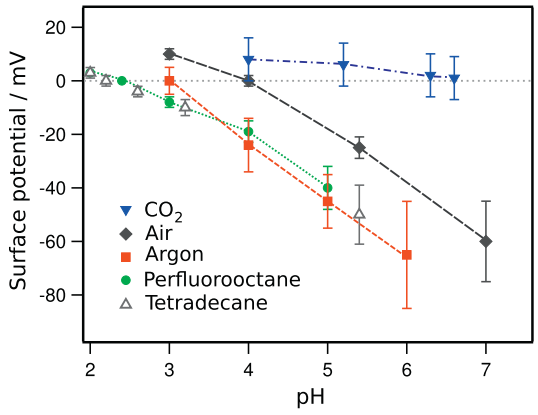

Fig. 4. Surface potentials as a function of pH for various gas bubbles and oil droplets determined from AFM experiments. Data is redrawn from Refs. [51,82].

gained on their stability or coalescence behaviour, and that this measurement is obtained directly as a function of separation.

The understanding gained from experimental measurements of bubble systems, coupled with analysis using the Chan–Dagastine–White model [16,18,20], allows a 'stability map' for bubbles to be generated. This shows the critical force required to induce coalescence for a pair of bubbles of given size at a certain pH, and such a map for air bubbles is shown in Fig. 5. Away from the isoelectric point (pH 4) at which all bubbles are unstable, larger bubbles require a larger applied force to induce coalescence under quasi-equilibrium conditions.

Because of their different isoelectric points, air bubbles and oil droplets experience a small window (around pH 2.5–4) wherein their surface charges are different, and hence where bubble–drop interactions are attractive [82]. By choosing oils which have a refractive index greater than water (e.g. hydrocarbons) or less than water (e.g. some fluorocarbons), similarly, the Van der Waals interaction can be either attractive or repulsive. This combination of effects means that pH and material choice can be used to control whether pairs of bubbles and droplets coalesce or not [82].

In addition to measuring the interactions between pairs of deformable bodies, bubbles and droplets can be used as probes for the surface properties of solid materials [41,87,88]. In this

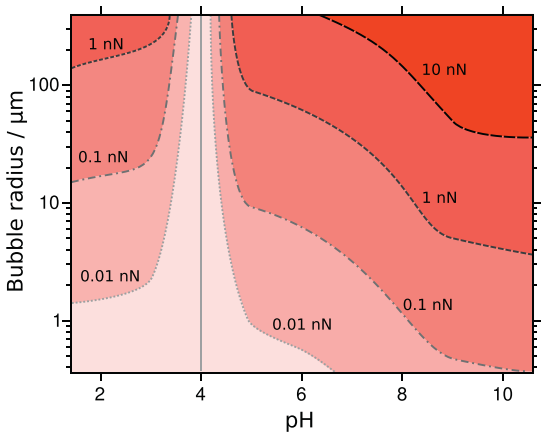

Fig. 5. A 'stability map' for air bubble–bubble interactions in aqueous solutions. The plot shows the critical force required in order for two bubbles to coalesce in an axisymmetric collision, in the absence of hydrodynamic effects. Data was obtained by using the Chan–Dagastine–White model [16,18].

capacity, their ability to increase their interaction area through deformation is particularly advantageous, allowing very sensitive measurements of low surface charges to be obtained. For example, the surface charging properties of native gold surfaces in both oxidised and unoxidised states, were measured by employing an air bubble as a probe [88]. This allowed an accurate map of the surface charging behaviour and the effect of the metastable surface oxide to be obtained. Interestingly, the iep of the gold surface moves significantly (from pH 4 to pH 6) on oxidation, giving new information on what a truly 'clean' gold surface means.

4.1.3. Non-DLVO forces: structural interactions

When colloidal additives such as micelles, polymer coils or nanoparticles are confined between two approaching surfaces, their presence influences the pressure experienced by the surfaces [89]. At low concentrations, this influence manifests as the well-documented depletion interaction, whereby exclusion of the additive at a certain separation induces a strong osmotic-based attraction between the surfaces. At higher concentrations of colloidal additive, alternating regions of attractive and repulsive pressure result from layers of the additive material being 'squeezed out' by the approaching surfaces. Such structural forces have been observed between solid surfaces for a range of additives, from micelles [90,91], polymers [92–94] and particles [95,96] to solvent molecules [97].

When confined between two deformable interfaces (such as oil–water or air–water boundaries), or between a solid surface and a deformable surface, the effects of such oscillating pressures are quite unexpected (Fig. 6). A strong hysteresis is seen between the forces experienced during approach and separation of the surfaces, linked specifically to deformation of the interface [52,98]. This hysteresis arises because of the coupled system of deformable structures – the AFM cantilever, and the droplet interface [56]. When the force gradient acting on the system exceeds the effective stiffness, the system can jump to the next stable position. This is the same reason that jumps to contact are seen in other AFM force experiments, e.g. when strong attractive Van der Waals forces occur between a tip and surface. The deformability of the surfaces provides an added degree of freedom for such jump instabilities to occur. By measuring the force between two rigid surfaces (such as a particle and a flat surface) immersed in a structured colloidal fluid, the disjoining pressure due to the structuring of the colloid can be obtained [52,98]. Using this as an input in the Chan–Dagastine–White model, it is possible to predict the force *vs.* separation relationship for the case of deformable bodies. Such model predictions are shown as solid and dotted lines in Fig. 6.

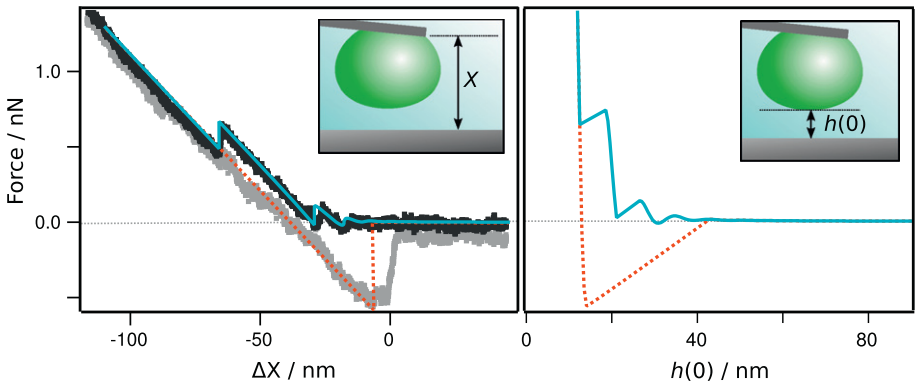

Fig. 6. Structural forces measured by the AFM between a drop of perfluorooctane and a mica surface in 400 mM SDS solution. The symbols are experimental data for approach (black) and retract (grey), and the lines are model fits for the approaching (solid) and retracting (dotted) interaction, obtained by using the Chan–Dagastine–White model [16,18]. Data is redrawn from Ref. [52].

It is seen that this hysteresis is linked to the radius of curvature and interfacial tension of the deformable interface (which together determine the deformability), and also to the size and concentration of the structuring colloid [52,98]. Broadly, a more deformable (less rigid) interface, or a smaller structuring colloid tends to favour strong hystersis, because of the sharper gradients in the force/separation profile. In such experiments, complementary anaylsis by small-angle neutron scattering (SANS) [99] has proven to be particularly advantageous in providing a method for analysing the size of, and interactions between the structuring colloidal additives [98,100].

4.1.4. Obtaining absolute separations in-situ

As mentioned in Section 2, one of the primary disadvantages of AFM when compared to, for example, SFA is that an absolute measurement of the separation between approaching interfaces is not known at all times. For the interaction of two solid bodies, this is not a significant problem, as the measurement can be calibrated from the point of hard contact. However, for interactions between deformable bodies where there is no point of hard contact, no such reference point is available, and the separation must either be determined theoretically, or by an additional measurement technique.

The first, indirect method, is through the application of the modelling framework [16–18] described in Section 4.1.1. In this case, the separation is found through fitting the model prediction to the experimental force/separation data. A good fit is only obtained when the spatial positioning predicted by the model and that within the experiment are identical, and hence the latter is derived.

Clark, Walz and Ducker used an evanescent wave-dynamic light scattering technique to deduce the separation between a silica particle and a planar surface during an AFM experiment [101]. However, this technique would be difficult to apply to a droplet or bubble system, particularly with the need to account for deformation.

Recently, laser scanning confocal microscopy was used to measure the initial separation between a drop and a surface, or between two drops, *in situ* before a dynamic AFM measurement [102] (Fig. 7). Comparison between this measurement and the prediction arrived at from application of the theoretical model to the subsequent AFM force/displacement data showed agreement to within 50 nm. The advantage of this technique is that is has wide applicability to any system that can be functionalised by addition of a fluorescence dye in order to highlight the relevant interfaces [103]. However, it is limited in terms of the drop sizes and geometries that can be explored, primarily due to lensing effects from the refractive index difference between oil and water. Methods to avoid this by index matching have been suggested [102].

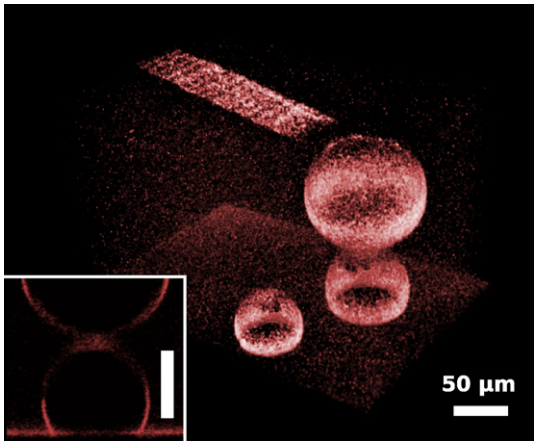

Fig. 7. 3-Dimensional reconstruction obtained by laser scanning confocal microscopy, taken *in situ* in the AFM, just prior to a drop-drop interaction measurement. The inset shows a vertical 'slice' through the image, precisely half way through the two aligned drops. Data is redrawn from Ref. [102].

4.2. Dynamic measurements – hydrodynamic effects

4.2.1. Modelling framework

In operating the AFM in a dynamic mode, relative displacement, Z (see Fig. 2a) of the cantilever is varied with time in a predetermined manner [17,18]. The measured force will now reflect a corresponding time variation. If the instantaneous separation between the interacting bodies are known, the force can be regarded as a function of separation even though both quantities will be time dependent in such dynamic experiments. Although expressing the (time dependent) force as a function of the (time dependent) separation means the dynamic results can be cast into a similar form to those in equilibrium measurement, this can end up masking new physical insight and potentially lead to mis-interpretation of key physical phenomenon. On the other hand by exhibiting how the force varies with time we can sometimes obtain a clearer physical understanding of the system behaviour. Furthermore, the capacity to vary the form of the relative displacement, for example, by changing the velocity at which the interacting bodies are pushed together and then separated, provides an additional avenue by which to probe the interaction and places stronger constraints on the way the interaction needs to be modelled [17–19].

It is important to note here that we are interested in interactions at nanometre separations between drops of tens of micrometres radius. On this scale, only two drops can interact at any one

time, as the drops are 'touching' or 'in contact' on the scale of the drop radii, which is commonly known as the lubrication approximation [17,18]. The many-body hydrodynamic interactions experienced at ranges on the order of the droplet radii are significantly weaker, and not dealt with here.

When the interacting bodies can deform, their shapes will also change with time and with this the effective area of interaction during the course of the interaction. This behaviour can be exploited to increase the sensitivity in measuring disjoining pressures. As we have seen in Section 4.1.3, such deformations were responsible for jump hysteresis events in the force curve that do not occur with rigid systems. From a modelling point of view, a model that accounts for the time variations of the force should also be capable of predicting the space and time dependent surface deformations.

In the context of dynamic AFM measurements in liquid systems, it is instructive to obtain estimates of the relative magnitudes of forces due to inertia, viscosity, surface tension (or capillarity) as well as possible time dependent processes due to material transport.

The first consideration in any hydrodynamic problem is to estimate the relative importance of inertia versus viscous effects. In typical AFM experiments, the cantilever is driven no faster than $V \approx 100$ μm/s and the bubble/drop radius would be below $R \approx 100$ μm. For water at a density of $\rho \approx 1000$ kg/m^3 and viscosity of $\mu \approx 10^{-3}$ Pa s, the effects of inertia to viscosity is measured by the Reynolds number, $Re = \rho RV/\mu \approx 10^{-2}$. Since it is small compared to unity, the interaction is viscosity dominated and hydrodynamic interactions can be treated in the low Reynolds number or Stokes flow regime.

The distortion of the surfaces of bubbles/drops by viscous forces is opposed by the surface tension. The ratio of the viscous to surface tension forces is characterised by the capillary number, $Ca = \mu V/\sigma$. For typical fluids, with surface tension, $\sigma \approx 50$ mN/m, we find $Ca \approx 10^{-5}$. In other words, surface tension forces are large compared to hydrodynamic forces. As such, one would expect that viscous deformation of bubbles/drops in AFM interactions can be described by the equilibrium Young–Laplace equation that describes how surfaces assume shapes that will minimise the interfacial area.[2]

The familiar disjoining pressure due, for example, to Van der Waals and electrical double layer that varies with interfacial separation also contribute to distorting the bubble/drop surfaces and hence to the force acting between them. Van der Waals forces that originate in the main from the quantum fluctuations of the electromagnetic field localised around the interface region between the interacting bubbles/drops will accommodate the change in local geometry effectively instantaneously. Changing the interfacial geometry also affects the state of the diffuse double layer and potentially affecting the electrical double layer interaction. However, ionic motion is sufficiently fast, taking only of the order 10^{-8} s for the ions in the diffuse double layer to re-adjust [104] so equilibrium expressions for double layer contribution to the disjoining pressure can be used in modelling.

The thickness of the film between interacting deformable bubbles/drops is small (≈nm) compared to the typical dimensions of the bubbles/drops (≈10 s of μm). Consequently, the film thinning process can be described by the Stokes–Reynolds lubrication theory. For a film with an axially symmetric thickness, $h(r,t)$ the film thinning equation [19] has the form

$$\frac{\partial h}{\partial t} = \frac{1}{12\mu r}\frac{\partial}{\partial r}\left(rh^3\frac{\partial p}{\partial r}\right) \tag{11}$$

where $p(r,t)$ is the hydrodynamic pressure within the film relative to the bulk solution. Implicit in the formulation of Eq. (11) is the assumption that the hydrodynamic boundary condition at the surfaces of deformable bubbles/drops obey the tangentially immobile boundary condition, the same as that at a solid surface. At the interface between pure fluids, it is generally assumed that the hydrodynamic boundary condition is the continuity of tangential stress. However, in all force measurement experiments for which we can make quantitative comparisons, the results are consistent with the tangentially immobile condition.

The local spatial variations of the thickness of the film can be related to the disjoining pressure, Π and the hydrodynamic pressure, $p(r,t)$ by the Young–Laplace equation:

$$\frac{\sigma}{nr}\frac{\partial}{\partial r}\left(r\frac{\partial h}{\partial r}\right) = \frac{2\sigma}{R} - (p + \Pi) \tag{12}$$

For the interaction between a solid sphere of radius, R_S and a deformable drop that possesses interfacial tension, σ and Laplace pressure of $(2\sigma/R_L)$, the constant $n = 1$, and $1/R = (1/R_s + 1/R_L)$. For the interaction between two bubbles/drops of interfacial tensions, σ_1 and σ_2, with Laplace pressures $(2\sigma/R_{L1})$ and $(2\sigma/R_{L2})$, the constant $n = 2$, and $2/R = (1/R_{L1} + 1/R_{L2})$, $2/\sigma = (1/\sigma_1 + 1/\sigma_1)$. Eqs. 11 and 12 constitute the Stokes–Reynolds–Young–Laplace (SRYL) model for the spatial and temporal evolution of the film thickness, $h(r,t)$. The time-dependent force, $F(t)$ can be calculated from the integral

$$F(t) = 2\pi\int_0^\infty [p(h(r,t)) + \Pi(h(r,t))]rdr \tag{13}$$

The SRYL equations have to be solved with the initial condition

$$h(r, t=0) = h_{init} + \frac{nr^2}{2R} \tag{14}$$

where h_{init} is the initial distance of closest approach between the interacting bodies. Its value, though cannot be measured directly, can be estimated accurately by a number of different ways (see Section 4.1.4). The choice of an initial quadratic shape for the film reflects the assumption that the initial undeformed shapes are locally spherical.

In practice, the SRYL equations are solved in the domain $0 \leqslant r \leqslant r_{max}$. Symmetry considerations give the conditions at the axis of symmetry $r = 0$:

$$\frac{\partial h(r,t)}{\partial r} = 0 = \frac{\partial p(r,t)}{\partial r} \quad \text{at } r = 0 \tag{15}$$

Outside the film as $r \to \infty$, the deformation is expect to vanish and this gives the limiting form: $p(r,t) \to 1/r^4$. Technically this is more conveniently implemented as:

$$\frac{\partial p(r,t)}{\partial r} + \frac{4}{r}p(r,t) = 0 \quad \text{at } r = r_{max} \tag{16}$$

The way in which the cantilever is driven in an AFM experiment enters via the boundary condition at r_{max}. For a particle-bubble/drop interaction, this condition is:

$$\frac{\partial h(r_{max},t)}{\partial r} = \frac{dZ(t)}{dt} + \frac{1}{K}\frac{dF(t)}{dt} - \frac{1}{2\pi\sigma} \times \frac{dF(t)}{dt}\left[\log\left(\frac{r_{max}}{2R_L}\right) + B(\theta)\right] \tag{17}$$

The time-dependent cantilever drive velocity is given by the function dZ/dt (see Fig. 2a). The effect of the rate of change of cantilever deflection is accounted for by the term $(1/K)(dF/dt)$ and the final term accounts for effects due to deformations of the bubble/drop.

[2] A more detailed argument that involves considering the capillary wave velocity and the relative speed between the interacting bubbles/drops reaches the same conclusion that the equilibrium Young–Laplace equation can be used to describe drop deformations [19].

The function $B(\theta)$ is given by Eq. (6) or (7). For the case of two interacting deformable bubbles/drops, the condition at r_{max} is:

$$\frac{\partial h(r_{max},t)}{\partial r} = \frac{dZ(t)}{dt} + \frac{1}{K}\frac{dF(t)}{dt} - \frac{1}{2\pi\sigma_1} \times \frac{dF(t)}{dt}\left[\log\left(\frac{r_{max}}{2R_{L1}}\right) + B(\theta_1)\right] - \frac{1}{2\pi\sigma_2} \times \frac{dF(t)}{dt}\left[\log\left(\frac{r_{max}}{2R_{L2}}\right) + B(\theta_2)\right] \quad (18)$$

with separate terms to account for deformations on each of the bubbles/drops.

The complexity of the SRYL system of equations reflects the fact that to describe the time-dependent interaction between deformable bodies, one needs a description of the hydrodynamic forces that for this case is given by the Stokes-Reynolds equation. Such forces, together with the separation dependent disjoining pressure will act to deform the bodies. Therefore a quantitative characterisation of how the bodies deform under externally applied forces is also needed. For bubbles/drops, this is given by the Young–Laplace equation. For a consistent and complete description, the force and the deformations must be calculated together.

4.2.2. Dynamic interactions between drops and bubbles using AFM

Measuring drop and bubble interactions at higher velocities has allowed an understanding of the hydrodynamic forces that act during such collisions to be obtained [10,15,41,43,82]. Initial work with hydrocarbon droplets in aqueous surfactant solutions demonstrated that the forces observed were highly dependent on interaction velocity [15], and these experiments and their analysis have informed subsequent measurements.

It is seen that when two drops begin to approach each other at speed, there is a resistance to their approach that is seen as a repulsive force. This results from hydrodynamic resistance in the intervening film which is generated between them. As they are pushed together more closely, this film thins, and surface forces become important [18,19]. If a repulsion dominates, the film will usually remain intact, but if an attractive force dominates, then coalescence may occur depending to what extent the film has thinned, and on its profile.

Similarly, when two drops are pulled apart from close approach, a negative force is seen, corresponding to an attraction. This force comes from the hydrodynamic 'suction' that results from the resistance to liquid re-entering the thin film. The extent of this attraction depends on the rate at which the droplets are pulled apart, and on how thin the film was before retraction began [19].

Since these initial experiments, a wide spectrum of dynamic interactions in soft matter systems have been observed with AFM. These have included oil droplet collisions in surfactant-free solutions [43,102], air bubble collisions with [49] and without [42] surfactant, bubble–solid interactions [41,50] and hetero-collisions between air bubbles and oil droplets [82]. In all of these examples, the simple hydrodynamic model presented above, based on the Stokes-Reynolds drainage and the Young–Laplace relation, is sufficient to interpret all of the experimental results.

Interestingly, in all of the cases mentioned above, a no-slip (immobile) boundary condition for the air–water and oil–water interfaces is seen. This is expected in the case when surfactants are adsorbed, but for bubbles or droplets in pure water or salt solutions, this seems to controvert conventional wisdom. A recent potential explanation for this seeming incongruity was presented by Browne, et al. who suggested that ion pairs may adsorb at interfaces [105], causing tangentially immobile boundary conditions via induced surface tension gradients.

4.2.3. Cantilever drag and viscosity

In the formulation of dynamic interactions under the Stokes–Reynolds–Young–Laplace (SRYL) model in Section 4.2.1, the only property of the cantilever we considered is its effective spring constant. The deflection of the cantilever is assumed to arise from forces that are acting on the particle or bubble/drop attached to the tip of the cantilever. However, when the cantilever is driven at high speeds and/or when the viscosity of the medium is high, cantilever deflection due to hydrodynamic drag as a result of its motion needs to be included in the analysis [106].

Under the low Reynolds number Stokes flow regime, we expect this additional deflection, S_{drag} will be proportional to the cantilever drive velocity, dZ/dt, the viscosity, μ and inversely proportional to the cantilever spring constant, K:

$$S_{drag} = -C\frac{\mu}{K}\frac{dZ(t)}{dt} \quad (19)$$

The sign convention is such that a positive value of S_{drag} corresponds to an apparent repulsion. This additional drag enters the SRYL model via the boundary condition at the end of the solution domain r_{max}. The term that accounts for the rate of change of cantilever deflection in Eqs. (17) and (18) has to be replaced thus

$$\frac{1}{K}\frac{dF(t)}{dt} \rightarrow \frac{1}{K}\frac{dF(t)}{dt} - C\frac{\mu}{K}\frac{d^2Z(t)}{dt^2} \quad (20)$$

in order to take into account cantilever deflection due to hydrodynamic drag.

The constant, C can be determined from the force curve at large separations when drop deformation is negligible and its value will depend only on the geometric properties of the cantilever. If data is available at different drive velocities, the value of C can be fitted to one velocity and should then be valid to characterise drag on the same cantilever at other velocities. Thus C is not a free fitting parameter of the system. For the type of cantilevers that we used [106], we found $C \approx 6 \times 10^{-3}$ m.

4.3. Understanding coalescence events

4.3.1. Coalescence in dynamic systems

By using air bubbles in high-salt aqueous solutions, Vakarelski et al. were able to demonstrate that during dynamic interactions, there are a number of different ways in which coalescence can occur [42]. In this system, the repulsive electrical double-layer forces are effectively sequestered by the high ionic strength, and so the only remaining surface force in the system is the Van der Waals attraction. Coalescence can occur when the film between bubbles thins sufficiently to allow this attraction to take over. However, the mechanism by which this occurs can differ depending on how the interaction occurs.

A simple method to induce coalescence is to push the bubbles together indefinitely – at some point, the film between them thins sufficiently to cause rupture and coalescence. Alternatively, the bubbles can be pushed to a certain, low applied force and held in position (often known as a 'dwell' in AFM experiments). This waiting period allows time for the film to drain, and hence coalescence to occur without the bubbles being pushed closer together any further.

Perhaps less intuitively, if bubbles are pushed together to a fixed force such that coalescence does not occur, then in some circumstances, they may coalesce *as they are pulled apart*. This is because the hydrodynamic suction effect on retraction means that the thinnest film is attained during this stage of the interaction. This phenomenon also explains coalescence in extensional flows for microfluidic devices [107,108].

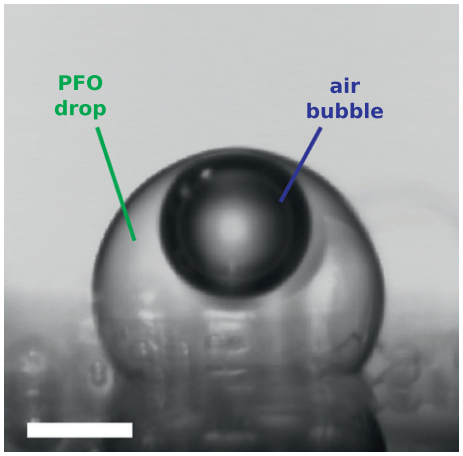

Fig. 8. The end result of a hetero-coalescence event between a perfluorooctane (PFO) droplet that originated on the substrate and an air bubble that originated on the cantilever. The scale bar represents 100 μm.

Another method to achieve coalescence is to bring the bubbles together sufficiently slowly that hydrodynamic resistance to drainage is insignificant. In this case, the interaction occurs under quasi-equilibrium conditions, where only surface forces are important. For the case mentioned above, where only an attractive Van der Waals force acts between the bubbles, this inevitably results in coalescence [51].

4.3.2. Homo- and hetero- pairs of bubbles and droplets

When two like fluid bodies coalesce (for example two bubbles, or two like droplets), the resultant body is a single, continuous bubble or droplet, with a volume comprising the sum of the inital two discrete bodies. However, for hetero interactions, where the two deformable bodies are not miscible (for example a gas bubble and an oil droplet, or a hydrocarbon and fluorocarbon oil droplet), then the result of coalescence is more complex. In this case, the bodies form a composite structure, conceptually similar to a floating oil lens at a planar air–water interface, where there may be any combination of air–water, oil–water and air–oil interface [82] (Fig. 8). Such paired systems have interesting possiblities for synthesis of asymmetric micro- or nano-scale objects and arrays, and have also found use in microfluidic logic circuits [109,110].

5. Conclusions and outlook

The analysis of interactions between soft materials by atomic force microscopy, and in particular bubbles and drops, has become a vital tool for the modern colloid scientist. Whereas such measurements present complex challenges, in terms of understanding the interplay of surface forces, deformation and absolute separations, significant insight has been gained through careful experimental design [15,49] and theoretical analysis and modelling [18,19]. Measurements of both static and dynamic interactions between homo- and hetero-pairs of bubbles [41,42,51,82], droplets [15,43,102] and particles [11] have been made and understood in terms of the fundamental forces and lubrication theories.

The fact that such progress has been made in the 20 years since the first colloidal AFM measurement suggests that this approach provides insight that is unique, but which complements that gained through other techniques. Fundamental studies have provided an understanding of when and how coalescence can occur in bubble systems [42], the unexpected charging properties of the bare oxidised gold surfaces used in almost all electronic devices [88], and the crucial role of CO_2 in air bubble stability [51], with potential implications for oceanic aerosol. Additionally, such experiments and studies have informed formulation of emulsions and foams for cosmetics, food and mineral processing, and are now helping in the understanding of new fields such as microfluidic drop manipulation [111]. Through understanding surface forces and hydrodynamics, dispersions with enhanced stability or shelf-life, and desirable rheological properties can be designed [52,98].

Interestingly, the current understanding of drops and bubbles appears comprehensive in some aspects, and yet progress to date has only addressed a fraction of the challenges in soft systems. The field of measuring such soft matter interactions is now sufficiently mature and developed that the pressing, unanswered questions of colloid science can, and should, be tackled. Examples might include the ubiquitous and as yet unexplained 'specific ion effect' [112], problems in high volume fraction emulsions and foams [113] (encouraged by increasing water scarcity), systems where molecular transport occurs and non-Newtonian fluids [114].

Acknowledgment

The authors would like to express their gratitude to co-workers, both past and present, who have provided much of the data and insight which has supported this work: T. Chau, R. Manica, I. Vakarelski, G. Webber, H. Lockie, O. Manor, C. Wu, E. Klaseboer. X. S. Tang and S. O'Shea are thanked for preparing the cantilevers used in many of the experiments. The ARC is thanked for financial support, and the Particulate Fluids Processing Centre, a special research centre of the ARC, provided infrastructure support.

References

[1] G. Binnig, C.F. Quate, C. Gerber, Phys. Rev. Lett. 56 (1986) 930.
[2] H.-J. Butt, Biophys. J. 60 (1991) 1438.
[3] W.A. Ducker, T.J. Senden, Langmuir 8 (1992) 1831.
[4] J.N. Israelachvili, D. Tabor, Proc. R. Soc. Lond. A 331 (1972) 19.
[5] H.-J. Butt, J. Colloid Interface Sci. 166 (1994) 109–117.
[6] W.A. Ducker, Z.G. Xu, J.N. Israelachvili, Langmuir 10 (1994) 3279.
[7] M. Preuss, H.-J. Butt, Langmuir 14 (1998) 3163.
[8] M.L. Fielden, R.A. Hayes, J. Ralston, Langmuir 12 (1996) 3721.
[9] B.A. Snyder, D.E. Aston, J.C. Berg, Langmuir 13 (1997) 590.
[10] D.E. Aston, J.C. Berg, Ind. Eng. Chem. Res. 41 (2002) 389.
[11] R.R. Dagastine, D.C. Prieve, L.R. White, J. Colloid Interface Sci. 269 (2004) 84.
[12] P. Mulvaney, J.M. Perera, S. Biggs, F. Grieser, G.W. Stevens, J. Colloid Interface Sci. 183 (1996) 614.
[13] D.E. Aston, J.C. Berg, J. Colloid Interface Sci. 235 (2001) 162.
[14] P.G. Hartley, F. Grieser, P. Mulvaney, G.W. Stevens, Langmuir 15 (1999) 7282.
[15] R.R. Dagastine, R. Manica, S.L. Carnie, D.Y.C. Chan, G.W. Stevens, F. Grieser, Science 313 (2006) 210.
[16] D.Y.C. Chan, R.R. Dagastine, L.R. White, J. Colloid Interface Sci. 236 (1) (2001) 141.
[17] R. Manica, J.N. Connor, R.R. Dagastine, S.L. Carnie, R.G. Horn, D.Y.C. Chan, Phys. Fluid 20 (3) (2008) 032101.
[18] D.Y.C. Chan, R. Manica, E. Klaseboer, Soft Matter 7 (2011) 2235.
[19] D.Y.C. Chan, E. Klaseboer, R. Manica, Adv. Colloid Interface Sci. 165 (2011) 70.
[20] R.R. Dagastine, L.R. White, J. Colloid Interface Sci. 247 (2) (2002) 310.
[21] D. Tabor, R.H. Winterton, Nature 219 (1968) 1120.
[22] D. Tabor, R.H. Winterton, Proc. R. Soc. Lond. A 312 (1969) 435.
[23] J.N. Israelachvili, D. Tabor, Proc. R. Soc. Lond. A 331 (1972) 19.
[24] J.N. Israelachvili, G.E. Adams, J. Chem. Soc., Faraday Trans. I 74 (1978) 975.
[25] J.N. Israelachvili, Intermolecular and Surface Forces, Academic Press, San Diego, 1991.
[26] R.G. Horn, D.J. Bachmann, J.N. Connor, S.J. Miklavcic, J. Phys. Condens. Matter 8 (1996) 9483.
[27] J.N. Connor, R.G. Horn, Faraday Discuss. 123 (2003) 193.
[28] R.A. Pushkarova, R.G. Horn, Langmuir 24 (2008) 8726.
[29] L.R. Fisher, E.E. Mitchell, D. Hewitt, J. Ralston, J. Wolfe, Coll. Surf. 52 (1991) 163.
[30] L.R. Fisher, D. Hewitt, E.E. Mitchell, J. Ralston, J. Wolfe, Adv. Colloid Interface Sci. 39 (1992) 397.
[31] R. Manica, D.Y.C. Chan, Phys. Chem. Chem. Phys. 13 (2011) 1434.
[32] E. Klaseboer, J.P. Chevaillier, C. Gourdon, O. Masbernat, J. Colloid Interface Sci. 229 (2000) 274.
[33] R. Manica, E. Klaseboer, D.Y.C. Chan, Soft Matter 4 (2008) 1613.
[34] V. Bergeron, C.J. Radke, Langmuir 8 (1992) 3020.

[35] D. Exerowa, D. Kashchiev, D. Platikanov, Adv. Colloid Interface Sci. 40 (1992) 201.
[36] V. Bergeron, J. Phys. Condens. Matter 11 (1999) 215.
[37] A. Sheludko, Adv. Colloid Interface Sci. 1 (1967) 391.
[38] K.J. Mysels, M.N. Jones, Discuss. Faraday Soc. 42 (1966) 42.
[39] D.C. Prieve, F. Luo, F. Lanni, Faraday Discuss. 83 (1987) 297.
[40] D.C. Prieve, Adv. Colloid Interface Sci. 82 (1999) 93.
[41] O. Manor, I.U. Vakarelski, G.W. Stevens, F. Grieser, R.R. Dagastine, D.Y.C. Chan, Langmuir 24 (20) (2008) 11533.
[42] I.U. Vakarelski, R. Manica, X. Tang, S.J. O'Shea, G.W. Stevens, F. Grieser, R.R. Dagastine, D.Y.C. Chan, Proc. Natl. Acad. Sci. USA 107 (2010) 11177.
[43] H.E. Lockie, R. Manica, G.W. Stevens, F. Grieser, D.Y.C. Chan, R.R. Dagastine, Langmuir 27 (2011) 2676.
[44] G.B. Webber, G.W. Stevens, F. Grieser, R.R. Dagastine, D.Y.C. Chan, Nanotechnology 19 (2008) 105709.
[45] J.P. Cleveland, S. Manne, D. Bocek, P.K. Hansma, Rev. Sci. Instrum. 64 (1993) 403.
[46] J.E. Sader, I. Larson, P. Mulvaney, L.R. White, Rev. Sci. Instrum. 66 (1995) 3789.
[47] R. Levy, M. Maaloum, Nanotechnology 13 (2002) 33.
[48] J.L. Hutter, J. Bechhoefer, Rev. Sci. Instrum. 64 (7) (1993) 1868–1873. ISSN: 0034.
[49] I.U. Vakarelski, J. Lee, R.R. Dagastine, D.Y.C. Chan, G.W. Stevens, F. Grieser, Langmuir 24 (3) (2008) 603.
[50] R.F. Tabor, R. Manica, D.Y.C. Chan, F. Grieser, R.R. Dagastine, Phys. Rev. Lett. 106 (2011) 064501.
[51] R.F. Tabor, D.Y.C. Chan, F. Grieser, R.R. Dagastine, Angew. Chemie Int. Ed. 50 (2011) 3454.
[52] R.F. Tabor, D.Y.C. Chan, F. Grieser, R.R. Dagastine, J. Phys. Chem. Lett. 2 (2011) 434.
[53] R.J. Hunter, Foundations of Colloid Science, second ed., Oxford University Press, Oxford, 2001.
[54] A.P. Gunning, A.R. Mackie, P.J. Wilde, V.J. Morris, Langmuir 20 (2004) 116.
[55] R.F. Tabor, S. Gold, J. Eastoe, Langmuir 22 (2006) 963.
[56] D. Bhatt, J. Newman, C.J. Radke, Langmuir 17 (1) (2001) 116.
[57] D.C. Bardos, Surf. Sci. 517 (2002) 157.
[58] W.A. Ducker, T.J. Senden, R.M. Pashley, Langmuir 8 (1992) 1831.
[59] I. Larson, C.J. Drummond, D.Y.C. Chan, F. Grieser, J. Am. Chem. Soc. 115 (1993) 11885.
[60] J.N. Israelachvili, R.M. Pashley, Nature 300 (1982) 341.
[61] A. Grabbe, R.G. Horn, J. Colloid Interface Sci. 157 (1993) 375.
[62] A.P. Legrand (Ed.), The Surface Properties of Silicas, John Wiley, New York, 1998.
[63] C.J. van Oss, J. Molec. Recog. 16 (2003) 177.
[64] Y.S. Djikaeva, E. Ruckenstein, J. Chem. Phys. 130 (2009) 124713.
[65] T.D. Blake, J.A. Kitchener, J. Chem. Soc., Faraday Trans. 1 (68) (1972) 1453.
[66] H.K. Christenson, J.F. Fang, B.W.a. Ninham, J. Phys. Chem. 94 (1990) 8004.
[67] E.E. Meyer, J.K. Rosenberg, J.N. Israelachvili, Proc. Natl. Acad. Sci. USA 103 (2006) 15739.
[68] J. Eastoe, C. Ellis, Adv. Colloid Interface Sci. 134–135 (2007) 89.
[69] V.S.J. Craig, B.W. Ninham, R.M. Pashley, Langmuir 15 (1999) 1562.
[70] V.S.J. Craig, J. Colloid Interface Sci. 183 (1996) 260.
[71] J.C. Eriksson, U. Henriksson, Langmuir 23 (2007) 10026.
[72] P. Attard, Langmuir 16 (2000) 4455.
[73] R.R. Dagastine, D.C. Prieve, L.R. White, J. Colloid Interface Sci. 231 (2) (2000) 351.
[74] V.A. Parsegian, G.H. Weiss, J. Colloid Interface Sci. 81 (1) (1981) 285.
[75] D.B. Hough, L.R. White, Adv. Colloid Interface Sci. 14 (1980) 3.
[76] D.C. Prieve, W.B. Russel, J. Colloid Interface Sci. 125 (1988) 1.
[77] L. Bergstrom, Adv. Colloid Interface Sci. 70 (1997) 125.
[78] C.J. Drummond, G. Georgaklis, D.Y.C. Chan, Langmuir 12 (1996) 2617.
[79] I.E. Dzaloshinskii, E.M. Lifshitz, L.P. Pitaerskii, Adv. Phys. 10 (1961) 165.
[80] S. Biggs, P. Mulvaney, J. Chem. Phys. 100 (1994) 8501.
[81] M.A. Bevan, D.C. Prieve, Langmuir 15 (1999) 7925.
[82] R.F. Tabor, C. Wu, H. Lockie, R. Manica, D.Y.C. Chan, F. Grieser, R.R. Dagastine, Soft Matter 7 (2011) 8977.
[83] J.K. Beattie, A.M. Djerdjev, Angew. Chemie Int. Ed. 43 (2004) 3368.
[84] P. Creux, J. Lachaise, A. Graciaa, J.K. Beattie, A. Djerdjev, J. Phys. Chem. B 113 (2009) 14146.
[85] M. Takahashi, J. Phys. Chem. B 109 (2005) 21858.
[86] J.F. Harper, J. Fluid Mech. 581 (2007) 157.
[87] O. Manor, I.U. Vakarelski, X. Tang, S.J. O'Shea, G.W. Stevens, F. Grieser, R.R. Dagastine, D.Y.C. Chan, Phys. Rev. Lett. 101 (2) (2008) 024501.
[88] R.F. Tabor, A.J. Morfa, F. Grieser, D.Y.C. Chan, R.R. Dagastine, Langmuir 27 (2011) 6026.
[89] D.T. Wasan, A.D. Nikolov, F. Aimetti, Adv. Colloid Interface Sci. 108–109 (2004) 187.
[90] D.L. Sober, J.Y. Walz, Langmuir 11 (1995) 2352.
[91] C.E. McNamee, Y. Tsujii, H. Ohshima, M. Matsumoto, Langmuir 20 (2004) 1953.
[92] A. Sharma, S.N. Tan, J.Y. Walz, J. Colloid Interface Sci. 191 (1997) 236.
[93] A.J. Milling, J. Phys. Chem. 100 (1996) 8986.
[94] S. Biggs, R.R. Dagastine, D.C. Prieve, J. Phys. Chem. B 106 (2002) 11557.
[95] A. Tulpar, P.R.V. Tassel, J.Y. Walz, Langmuir 22 (2006) 2876.
[96] M. Piech, J.Y. Walz, J. Colloid Interface Sci. 253 (2002) 117.
[97] R.G. Horn, J.N. Israelachvili, J. Chem. Phys. 75 (1981) 1400.
[98] R.F. Tabor, H. Lockie, D.Y.C. Chan, F. Grieser, I. Grillo, K.J. Mutch, R.R. Dagastine, Soft Matter 7 (2011) 11334.
[99] I. Grillo, Soft Matter Characterization, Springer, New York, 2008. Chapter: Small-Angle Neutron Scattering and Applications in Soft Condensed Matter, pp. 723–782.
[100] S.H.L. Klapp, Y. Zeng, D. Qu, R. von Klitzing, Phys. Rev. Lett. 100 (2008) 118303.
[101] S.C. Clark, J.Y. Walz, W.A. Ducker, Langmuir 20 (2004) 7616.
[102] R.F. Tabor, H. Lockie, D. Mair, R. Manica, D.Y.C. Chan, F. Grieser, R.R. Dagastine, J. Phys. Chem. Lett. 2 (2011) 961.
[103] J. Pawley, Handbook of Biological Confocal Microscopy, Springer, New York, 2006.
[104] J.T.G. Overbeek, J. Colloid Interface Sci. 58 (1977) 408.
[105] C. Browne, R.F. Tabor, D.Y.C. Chan, R.R. Dagastine, M. Ashokkumar, F. Grieser, Langmuir 27 (2011) 12025.
[106] R.R. Dagastine, G.B. Webber, R. Manica, G.W. Stevens, F. Grieser, D.Y.C. Chan, Langmuir 26 (2010) 11921.
[107] Z.D. Gunes, X. Clain, O. Breton, G. Mayor, A. Burbidge, J. Colloid Interface Sci. 343 (2010) 79.
[108] N. Bremond, A.R. Thiam, J. Bibette, Phys. Rev. Lett. 100 (2008) 024501.
[109] S.A. Khan, S. Duraiswamy, Lab Chip 9 (2009) 1840.
[110] S. Duraiswamy, S.A. Khan, Nano Lett. 10 (2010) 3757.
[111] K. Schoenwald, Z.C. Peng, D. Noga, S.R. Qiu, T. Sulchek, Rev. Sci. Instrum. 81 (2010) 053704.
[112] V.S.J. Craig, B.W. Ninham, R.M. Pashley, J. Phys. Chem. 97 (1993) 10192.
[113] V.O. Ikem, A. Menner, A. Bismarck, Angew. Chemie Int. Ed. 47 (2008) 8277.
[114] M.S. Barrow, W.R. Bowen, A. Hilal, N. abd Al-Hussany, P.R. Williams, R.L. Williams, C.J. Wright, Proc. R. Soc. Lond. A 459 (2003) 2885.